Published in final edited form as:
Adv Biosyst. 2019 February ; 3(2): . doi:10.1002/adbi.201800308.

The Axon Initial Segment is the Dominant Contributor to the Neuron's Extracellular Electrical Potential Landscape

Dr. Douglas J. Bakkum,
Department of Biosystems Science and Engineering, ETH Zurich, Mattenstrasse 26, CH-4058 Basel, Switzerland

Dr. Marie Engelene J. Obien,
Department of Biosystems Science and Engineering, ETH Zurich, Mattenstrasse 26, CH-4058 Basel, Switzerland; RIKEN Quantitative Biology Center, 2-2-3 Minatojima-minamimachi, Chuo-ku, Kobe 650-0047, Japan; MaxWell Biosystems AG, Mattenstrasse 26, CH-4058 Basel, Switzerland

Dr. Milos Radivojevic,
Department of Biosystems Science and Engineering, ETH Zurich, Mattenstrasse 26, CH-4058 Basel, Switzerland

Dr. David Jäckel,
Department of Biosystems Science and Engineering, ETH Zurich, Mattenstrasse 26, CH-4058 Basel, Switzerland; MaxWell Biosystems AG, Mattenstrasse 26, CH-4058 Basel, Switzerland

Dr. Urs Frey,
Department of Biosystems Science and Engineering, ETH Zurich, Mattenstrasse 26, CH-4058 Basel, Switzerland; RIKEN Quantitative Biology Center, 2-2-3 Minatojima-minamimachi, Chuo-ku, Kobe 650-0047, Japan; MaxWell Biosystems AG, Mattenstrasse 26, CH-4058 Basel, Switzerland

Prof. Hirokazu Takahashi, and
Research Center for Advanced Science and Technology, The University of Tokyo, 4-6-1 Komaba, Meguro-ku, Tokyo 153-8904, Japan

Prof. Andreas Hierlemann*
Department of Biosystems Science and Engineering, ETH Zurich, Mattenstrasse 26, CH-4058 Basel, Switzerland

Abstract

Extracellular voltage fields, produced by a neuron's action potentials, provide a widely used means for studying neuronal and neuronal-network function. The neuron's soma and dendrites are thought to drive the extracellular action potential (EAP) landscape, while the axon's contribution is usually considered less important. However, by recording voltages of single neurons in dissociated rat cortical cultures and Purkinje cells in acute mouse cerebellar slices through

andreas.hierlemann@bsse.ethz.ch.

Conflict of Interest
M.E.J.O. and U.F. are cofounders of MaxWell Biosystems AG, Mattenstrasse 26, c/o ETH Zurich, Basel 4058, Switzerland. D.J. is now employed at MaxWell Biosystems AG.

iDThe ORCID identification number(s) for the author(s) of this article can be found under https://doi.org/10.1002/adbi.201800308.

Europe PMC Funders Author Manuscripts

hundreds of densely packed electrodes, it is found, instead, that the axon initial segment dominates the measured EAP landscape, and, surprisingly, the soma only contributes to a minor extent. As expected, the recorded dominant signal has negative polarity (charge entering the cell) and initiates at the distal end. Interestingly, signals with positive polarity (charge exiting the cell) occur near some but not all dendritic branches and occur after a delay. Such basic knowledge about which neuronal compartments contribute to the extracellular voltage landscape is important for interpreting results from all electrical readout schemes. Finally, initiation of the electrical activity at the distal end of the axon initial segment (AIS) and subsequent spreading into the axon proper and backward through the proximal AIS toward the soma are confirmed. The corresponding extracellular waveforms across different neuronal compartments could be tracked.

Keywords

axon initial segment (AIS); extracellular action potential (EAP); high-density microelectrode array (HD-MEA); neurons; signal propagation

1 Introduction

The details of how different neuronal compartments (soma, axons, dendrites) and different cell types contribute to the extracellular action potential (EAP) in vitro were not yet demonstrated with direct experimental evidence. A variety of theoretical[1–4] and a number of experimental[5–10] studies address the subcellular origin of EAPs. In most reports, axonal contributions to the EAP have been considered negligible or small, possibly due to a notion that small cell compartments require less current to depolarize.[3,11] Along these lines, initial patch-clamp data show similar axon initial segment (AIS) and somatic sodium currents per area of membrane,[12] which are the currents responsible for action potential generation. In other words, the much larger soma would then produce a much greater cumulative current. On the other hand, immunohistological evidence shows that sodium channels are expressed to a much higher degree in the AIS.[13] There, they are tightly coupled to the actin cytoskeleton and not easily drawn into a patch pipette, which suggests that the initial patch-clamp data may underestimate sodium current at the AIS.[14] Quantitative freeze-fracture immunogold labeling,[15] outside-out patch-clamp recordings,[13] and experimentally constrained models[14] show that the AIS of pyramidal neurons has about 35 to 50 times higher sodium channel density than the soma or proximal dendrites. Likewise, while not focusing on the EAP, early modeling studies predict that a 20- to 500-fold higher density of sodium channels is necessary for action potentials to initiate in the AIS.[16,17] A simplistic calculation using a 50-fold increase shows that the AIS would indeed be able to influence the EAP: an AIS would have ≈5 times greater total sodium conductance than a soma, assuming a 17 μm diameter spherical soma and a 31 μm length cylindrical AIS (mean values from our data, which also matches ratios in ref. [17]) with an estimated 1 μm diameter; conductance is considered to be proportional to surface area multiplied by the channel density. However, whether or not the AIS has more sodium channels than the soma, and to what degree, remains debated.[12,18,19]

Europe PMC Funders Author Manuscripts

Here, we compared neurons' EAPs to fluorescence images of cell morphology in primary rat cortical cultures and acute mouse cerebellar slice preparations and present direct evidence that the EAP spatial distribution or landscape is dominated by the AIS, not the soma. The spatial distribution and strength of the EAP is related to the AIS geometry and degree of formation. Our results add experimental evidence into the debate about the distribution of sodium channels in a neuron. To gather the data, neurons' EAPs were recorded in high spatial detail by using custom microelectrode arrays containing 11011 densely packed electrodes (17.8 μm pitch; 8.2 × 5.8 μm^2 area per electrode; density of 3400 electrodes per mm^2).[20,21] Immediately after recording, cells were imaged in order to match which cell compartments contributed which features to the neurons' EAP landscape. For the primary cultures, spontaneous EAPs of single neurons were sampled at multiple locations simultaneously at two to three weeks in vitro; to minimize overlap of voltage signals in recordings and neurites in images between neighboring neurons, we grew low-density cultures that contained a few to tens of neurons per array. A glutamic acid decarboxylase 67-green fluorescent protein (GAD67-GFP) knock-in mouse line[22] that allowed for live imaging of Purkinje cells was used for acute slice recordings. For single-cell analysis in acute slices, we injected Lucifer yellow to obtain the morphology of the recorded Purkinje cells. We conclude the paper with a brief discussion about how our results can affect interpretations of extracellularly recorded electrophysiological data.

2 Results and Discussion

2.1 Extracellular Potential Landscape

Owing to the large electrode density, we were able to extracellularly capture the waveforms across all neuronal compartments, including axons and dendrites, at subcellular resolution, as can be seen in Figures 1 and 2. Typical monophasic large-amplitude negative signals were observed at the AIS, while biphasic and triphasic (positive-first) waveforms were observed along the axonal segments. Low-amplitude positive signals were detected in the dendritic regions. The largest extracellular signal spike always had negative polarity (Figure 1B) and was typically localized near the proximal AIS or the peak Ankyrin-G (AnkG; a molecular marker of the AIS) immunofluorescence signal (Figure 1A) but never at the soma (Figure 1C). Especially, the signals of cells, whose AIS originated from a dendrite (see Figure 1A bottom), clearly evidenced that the EAP was correlated with AIS location and shape. Signals near the soma of such cells typically were not detectable unless averaging multiple EAPs (Figure 1B bottom, electrode 5). An AIS was considered to have a dendritic origin, if it began at a neurite branch point, whose other branch expressed microtubule-associated protein 2 (MAP2; a molecular marker of somatodendritic regions) and not AnkG.

Out of the 49 neurons from 12 cultures (neurons that may have had overlapping voltage signals were excluded), 26 had an AIS with a dendritic origin, which is a common phenomenon observed in a variety of preparations.[23,24] As an "axon hillock" is not obvious for such cells, we define the "neck" as the distance from the proximal end of the AIS to the soma. The neck length was 31 ± 24 μm (mean ± s.d., $N = 26$) for AISs of dendritic origin and 7 ± 7 μm ($N = 23$) for AISs of somatic origin. A significant relationship

did not exist between the largest EAP spike and neck length (Pearson's correlation coefficient $r = 0.16$, $p = 0.27$, $N = 49$).

Moreover, EAP spike amplitude did not depend on whether the AIS was of somatic or dendritic origin ($p = 0.71$, two-side t-test, $N = 49$), which demonstrated that the relative location of the soma does not strongly influence the magnitude of the EAP. Importantly, AIS lengths were positively correlated to the spike amplitude ($r = 0.28$, $p = 0.05$, $N = 49$). The soma diameter was positively correlated to the largest EAP spike for AISs with somatic ($r = 0.47$, $p = 0.02$, $N = 23$) but not dendritic ($r = 0.06$, $p = 0.75$, $N = 26$) origins. Overall, AIS lengths and soma diameters were 31 ± 13 and 17 ± 5 μm, respectively (mean ± s.d., $N = 49$).

2.2 Initiation and Spreading of Extracellular Activity

In a next step, we looked at the initiation and spreading of the electrical activity of individual neurons and the corresponding extracellular waveforms across the different neuronal compartments at high spatiotemporal resolution.

Consistent with most reports in the literature, action potentials typically initiated at the distal AIS,[8,13,18,25,26] and EAP amplitude at the distal AIS was lower than the largest EAP (Figures 1C, 2, and 3A–D). Dual-patch recordings of soma and axon,[8,27] voltage sensitive dye recordings,[28] and modeling[8,14] show that action potentials initiate in the axon at about 40 μm from the soma. This is consistent with the location of the distal end of the AIS that we found for AISs originating from the soma (36 ± 13 μm, mean ± s.d.). Once initiated, action potentials propagated in both directions: into the axon proper and backward through the proximal AIS and toward the soma. This scenario holds for both cases of axons originating directly from the soma or from dendrites (Figure 2). While it is commonly assumed that the AIS extends over the very proximal portion of the axon that emerges from the soma at the axon hillock,[29] different axon onsets in various types of neurons have also been described.[23,30] Axons growing out of dendrites have been reported on in cortical neurons in primates[31] and cats.[32] Dendrites have been shown to serve as origin for axons in CA1 pyramidal neurons,[15] and for interneurons of different types, some of the latter having even more than one axon.[33]

Of the 22 neurons with an AIS length longer than 30 μm, the average propagation velocity from the distal initiation site to the proximal end of the AIS was 1.1 ± 1.5 m s^{-1} (mean ± s.d.; 65.6 μm median AIS length and 0.6 m s^{-1} median propagation velocity); the distal end of the AIS always fired first. The velocities were similar to those of action potentials propagating in unmyelinated cortical axons outside of the AIS that we have previously reported.[34] Some of the neurons with shorter AIS lengths showed action potentials occurring nearly simultaneously throughout the AIS or, in two cases, first at the proximal end of the AIS or at the soma (Figure 3D). For the 15 neurons with a neck length greater than 30 μm, the propagation velocity from the proximal AIS to the soma center was slower at 0.3 ± 0.2 m s^{-1} (mean ± s.d.; 0.2 m s^{-1} median).

2.3 Live-Cell Imaging and Patch Clamp

As a control, live-cell imaging and patch-clamp electrophysiology verified that the largest-amplitude extracellular action potential was spatially offset from the soma and distally

initiated (Figure 3E,F). Here, action potentials were evoked by applying current injection through the patch pipette. Results were consistent across five experiments. Alexa Fluor 594 dye was injected into the cell via the patch pipette in order to perform simultaneous live-cell imaging. The extracellular signal is approximately proportional to the negative derivative of the intracellular signal[6] (and is proportional to the membrane current).[1,4,6] Then the peak negative extracellular amplitude corresponds to the point of maximum positive slope on the intracellular trace (Figure 3F). The EAP is ≈2 orders of magnitude smaller than an intracellular AP. Therefore, periods of slower change in the intracellular AP correspond to a small or not detectable EAP. The initial positive deflection in the EAP near the soma is typical of capacitive membrane currents. These would be caused by intracellular currents, spreading axially from the AIS, charging the membrane prior to the opening of voltage-gated ion channels.

2.4 Regions of Positive-Amplitude Signals

While the largest amplitude spikes had negative polarity and were colocalized with AISs, spikes with positive polarity were colocalized with some, but not all, dendritic branches (Figure 4A; see also Movie S1 in the Supporting Information to get a better impression of the dynamics of the EAP landscape and signal spreading). The average peak negative spike was 6.9 times bigger than the average peak positive spike and 5.9 times bigger than the average somatic spike, which also had a negative polarity ($N = 24$) (Figure 4C). The colocalization of the positive peaks with dendrites and their mostly monophasic nature suggest that they are caused by a passive (i.e., capacitive) return current balancing the influx of sodium ions at the AIS. Alternatively, voltage-gated potassium channels that are expressed in dendrites could also be involved.[35] Interestingly, in our measurements (Figure 4B) we found a delay between the occurrence of negative and positive spikes: 113 ± 108 μs (mean ± s.d., 86 μs median, $N = 24$; see also Movie S1, Supporting Indormation). The delay was significantly correlated to the axial distance ($r = 0.79$, $p = 0.001$; Figure 4B) and not straight-line distance ($r = 0.34$, $p = 0.11$), suggesting an intracellular influence.[36] As the return currents, which are passive, capacitive currents drawn from the entire cell membrane upon Na^+-ion influx at the AIS, are key contributors to the positive signals, their amplitude depends on the resistance of the conducting path between the location of the Na^+-ion influx into the neuron (AIS) and the location of the measured return current. The extracellular path can be estimated to contribute only little to this resistance, as the medium resistance (saline) is comparably low, whereas the intracellular path, i.e., the resistance along the different dendritic branches may significantly vary (thickness and length) and, therefore, cause an uneven distribution. In addition, the return currents are significantly influenced by the local membrane capacitance (local specific membrane capacitance and membrane area), which also may add variability. Moreover, signals at dendritic locations will be influenced by other components, such as active ionic currents from nearby neurites and the presence of other cells, such as glia, that may affect resistivity. Likewise, how and why dendritic branches differentially contribute to the EAP (Figure 4A) is an important future study. For Figure 4, 25 of the 49 neurons were excluded, because either some distal parts of their dendritic arbor were not recorded at the same time as the AIS, or their dendritic arbor overlapped with neurites from another cell.

2.5 Measurements in Acute Slices

To investigate the role of the AIS also in neuronal tissue closely resembling in vivo morphology, we performed further experiments in Purkinje cells in acute cerebellar mouse slices (Figures 5 and 6). Purkinje cells differ from cortical neurons by having a more passive dendritic tree and larger soma. These two features would make it more likely that the largest extracellular signal would arise from the soma, if the soma instead of the AIS would be the source of the signal. Nevertheless, corroborating the results from cortical cell cultures above, the largest negative EAPs (Figure 5A) occurred in the area containing axons instead of at the Purkinje cell layer (i.e., the location of all Purkinje somas), and the positive EAPs (Figure 5B) consistently occurred in the area containing dendrites. In all cases, the largest negative EAPs were found to colocalize with the putative location of the Purkinje cell AISs; the mean of negative amplitudes peaked sharply ≈40 μm away from the center of the Purkinje cell layer, in the granular cell layer (Figure 5C). Moreover, we could again confirm the initiation of the action potential at the AIS (see also Figure 6C), which has been described in previous reports.[26]

On the other hand, the largest positive EAPs (i.e., the return currents) occurred 40–100 μm away from the center of the Purkinje cell layer, in the molecular layer. Purkinje cells have a stereotypical orientation: their AISs are always at the granular cell layer, between the white matter and the Purkinje cell layer; their dendritic arbors are located in the molecular layer, fanning out opposite the AIS from the Purkinje cell layer toward the pia. Parasagittal slices were made in order to keep the full morphology of Purkinje cells intact for recording. Purkinje cells are GABAergic and produce large spontaneous spikes even without synaptic input; the parallel fibers that would provide input get cut during slicing.

In order to then map the EAP distribution of individual in Purkinje cells to the respective cell morphology in the acute slice, we combined cell-attached patch-clamp with high-spatiotemporal-resolution microelectrode-array measurements (Figure 6). Purkinje cells were injected with Lucifer yellow, so that their exact position with respect to the electrodes could be visualized by combining fluorescence microscopy and differential-interference-contrast-microscopy (Figure 6A). We then determined the spatial distribution of ≈100 averaged spontaneous EAPs, while the timing of the action potentials was obtained through cell-attached patch-clamp. Again, the largest-amplitude EAPs were found along the axon at a distance of 20–40 μm from the soma (Figure 6B). The yellow line in Figure 6B marks the border between the molecular layer (ML) and the Purkinje cell layer (see also Figure 5A). The averaged EAPs obtained from the string of marked electrodes across the Purkinje cell and through cell-attached patch-clamp are shown in Figure 6C. As in the case of the dissociated cells, we recorded the largest-amplitude signals in the region of the putative AIS at considerable distance from the soma. The individual EAP traces of the electrodes, labeled 1–3 in Figure 6C, are shown in Figure 6D along with the average trace, the same holds for the cell-attached patch-clamp (top trace marked with a star). Finally, the effect is visualized in Figure 6E showing a side-view schematic of the Purkinje cell morphology, the estimated extracellular potential distribution and extracellular waveforms.

2.6 Discussion of the Results

The basic and fundamental observation of the EAP being driven by currents from the AIS instead of the soma can affect how extracellular recordings are interpreted. For example, neurons with spherically symmetric dendrites are thought to produce small EAPs due to the summation of dendritic membrane currents canceling each other out (axonal contributions presumed negligible).[9,37] However, such symmetry is broken when membrane currents originate from the AIS or from specific dendritic branches (Figure 4A). Likewise, neurons with smaller soma are thought to produce smaller EAPs,[11] but we observed this only for neurons with an AIS originating from the soma. Why wide variations in EAP waveforms exist between cells has been unclear[5] but can be explained to a degree by variations in AIS shape and level of AIS formation. In our preparation, EAP magnitudes reached up to 952 μV (even up to 1.8 mV in previous data[34]) and AIS lengths between 13 to 71 μm. “Silent” cells existed and were typically associated with decreased or no AnkG expression. Occasionally, AISs were forked, which produced distorted or double-spiked EAPs depending on the recording location. Why different dendritic branches produce different extracellular signals (cf. Figure 4A) is harder to explain and may require different experimental approaches to decipher. In tangential work, the AIS has been identified as the site with the lowest threshold and highest reliability for extracellular stimulation,[38,39] whereas stimulation under the soma often failed to evoke action potentials.[39] This finding supports the AISs significant contribution to the EAP and provides further indirect evidence that the AIS contains a higher concentration of voltage-gated ion channels.

The general phenomenon that the largest signal amplitudes occur in the region of the AIS is valid for in vitro situations and, most likely, also holds for in vivo situations, as can be concluded from the acute-slice measurements. The EAP arises from neuronal membrane currents, in particular from voltage-gated sodium channels. Previous studies showed that the molecular composition of axons in vitro and in vivo, including sodium channel distribution in the AIS, are consistent.[40] This implies that the membrane currents responsible for the EAP will likewise be similar. In turn, how the electric field spreads in the medium and is picked up as a potential on the recording electrodes depends on the specific recording scenario and is governed by laws of physics, i.e., Maxwell’s equations.[4] In other words, this aspect is largely independent of whether the experimental preparation is in vitro or in vivo. Nevertheless, we also experimentally addressed this issue and found consistent results in acute cerebellar slices, which preserve in vivo local microarchitecture (Figures 5 and 6). It is not expectable that ion-channel densities significantly change during the comparably short slice preparation.

Extracellular signal amplitudes in vitro and in vivo can be influenced by many factors, such as electrode impedance, the local microenvironment, or the degree of coupling between a neuronal membrane and an electrode. However, these influences likely had a negligible effect on our in vitro results. We deposited platinum black on the electrodes (see the Experimental Section). Besides reducing the electrode impedance, platinum black also reduces variations in signal amplitude due to impedance mismatches across the arrays’ electrodes to about 5%.[41] This variation is negligible when compared to the AIS-to-soma or AIS-to-dendrites signal amplitudes that differ by over 600% on average (Figure 4C).

Consistent results across 49 individual neurons and multiple preparations (cultured neurons and acute slices) provide strong evidence that the results were not an artifact from variations in local microenvironments or coupling. Further evidence is that a neuron's EAP is detected by multiple neighboring electrodes, including sites that are not immediately adjacent or coupled to a neuronal membrane, and that the signal attenuates with increasing distance from the source as expected (Figures 1A, 2A, 3E, and 4A). In summary, the AIS was found to dominate the extracellularly recorded electrical-potential distribution.

3 Conclusion

The neuron's soma and dendrites are commonly thought to give rise to its extracellular voltage signal, while signals from the axon are usually considered less important. Instead, we found that the largest amplitude of the extracellular signal originates from the AIS, not from the soma. These findings in cultures of dissociated primary rat cortical neurons were confirmed with recordings from Purkinje cells in acute cerebellar slices of mice. Our investigations show that changes in the AIS position and function can be observed in high spatiotemporal detail in vitro by means of high-density extracellular electrophysiology. Moreover, we confirmed initiation of the electrical activity at the distal end of the AIS and subsequent spreading into the axon proper and backward through the proximal AIS toward the soma. The involved specific extracellular waveforms could be tracked at high spatiotemporal resolution across the different neuronal compartments.

4 Experimental Section

Animal Use

Protocols were approved by the Basel Stadt veterinary office according to Swiss federal laws on animal welfare and the Animal Research Committee of the RIKEN Center for Developmental Biology.

Low-Density Cell Culturing

Cells from embryonic day 18 Wistar rat cortices were dissociated in trypsin, followed by mechanical trituration, and 1000 cells were seeded over an area of ≈4 mm^2 on top of the microelectrode arrays. Neurons and glia grew in 2 mL of serum-containing Neurobasal-based medium for 5 days. Thereafter, half of the medium was changed once a week to serum-containing Dulbecco's modified eagle medium. Detailed media recipes are available in ref. [34].

Immunocytochemistry

The neural source of extracellular signals was verified optically by immunocytochemistry performed immediately after a recording session. A detailed protocol is given in ref. [34]. The primary antibodies to microtubule-associated protein 2 (MAP2; Abcam ab5392; RRID:AB_2138153) and ankyrin-G (AnkG; NeuroMab clone N106/36; RRID:AB_10697718) were diluted 1:200 and left overnight at 4 °C on a shaker set to low speed. The secondary antibodies containing Alexa Fluor 647 (RRID:AB_10374876) or

Alexa Fluor 488 (RRID:AB_10561551) were diluted 1:200 and left for 1 h at room temperature in the dark.

Acute Cerebellar Slice Preparation

CD-1 or GAD67-GFP knock-in mice,[22] postnatal day 21–37, were obtained from the Laboratory for Animal Resources and Genetic Engineering in RIKEN Center for Developmental Biology Kobe, Japan. The mice were anaesthetized by isoflurane inhalation and then decapitated. The procedure for preparing cerebellar slices has been adapted from.[7] Briefly, the brain was dissected and immediately immersed in ice-cold carbogenated artificial cerebrospinal fluid (ACSF) containing in mm: NaCl 125, KCl 2.5, NaH_2PO_4 1.25, $MgSO_4$ 1.9, Glucose 20, $NaHCO_3$ 25. The cerebellum was separated from the cortex by cutting with a blade and glued onto a tray along its sagittal plane. Parasagittal cerebellar slices (150–200 μm thick) were obtained using a vibratome (Leica VT1200S). The slices were incubated at 35 °C in ACSF with 2 mM $CaCl_2$ for 30–45 min and then maintained at room temperature until recording. The slice was perfused with warm (≈33–35 °C), carbogenated ACSF throughout the recording.

Recording of EAPs with Complementary-Metal-Oxide-Semiconductor (CMOS)-Based Microelectrode Arrays

Cortical networks were grown for two to three weeks over 11011-electrode CMOS-based microelectrode arrays (1.8 × 2.0 mm^2 area containing 11000 8.2 × 5.8 μm^2 electrodes; 17.8 μm electrode pitch; 20 kHz sampling rate). Acute cerebellar slices were placed flat on the arrays and continuously superfused with carbogen-loaded ACSF (≈30–33 °C) throughout the experiment. See ref. [20] for circuit details of the CMOS-based microelectrode arrays. To identify the locations of the neurons growing over the array, a sequence of overlapping recording configurations was scanned across the array. A configuration is defined as how switches are set to connect a subset of the electrodes to the 126 available readout channels. Switches are reconfigurable within a few milliseconds. The largest possible contiguous block includes 6 × 17 electrodes, and 147 overlapping block configurations were used to scan the whole array at a rate of 1 min per configuration. A recording session lasted 2.5 h. Cell-culture recordings were acquired inside an incubator in order to control environmental conditions (36 °C and 5% CO_2).

Spatial and Temporal Signal Upsampling

Signals were upsampled to 160 kHz using the Nyquist-Shannon sampling theorem and the Whitaker-Shannon interpolation formula to improve temporal resolution.[42] The theorem is a mathematical proof that any sampled signal can be perfectly reconstructed into the original analog signal, as long as the analog signal has frequency components less than the Nyquist frequency. The microelectrode array circuitry filters the analog data with a first-order filter and an upper cutoff frequency of 3.7 kHz, before data are sampled at 20 kHz, which satisfies the requirements. To estimate waveforms between recording electrodes, upsampled and averaged EAPs were then spatially interpolated across a 1 × 1 μm^2 grid by cubic interpolation in Matlab (“griddata” function; MathWorks Matlab R2014a). Spatial estimation will introduce a measurement error that contributes to increased variation in the data. This error is accounted for in the error bars/variance presented in the figures and text.

Patch-Clamp Recording

Whole-cell patch-clamp was done on cells in cultures,[43] and cell-attached patch-clamp was performed on Purkinje cells in acute slices. The micropipettes had resistances of 5–7 MΩ. Micropipettes, used for whole-cell patch-clamp, were filled with internal solution (in mM): $C_6H_{11}KO_7$ 135, KCl 20, $MgCl_2 \cdot 6H_2O$ 2, HEPES 10, EGTA 0.1, Na_2ATP 2, Na_3GTP 0.3, adjusted to a pH of 7.3 with KOH. To image the cell, 0.02 mM Alexa Fluor 594 (Life Technologies) was added to the internal solution. Micropipettes used for cell-attached patch were filled with standard ACSF. A fluorescent dye, 2 mM Lucifer yellow CH (Sigma-Aldrich), was added for cell imaging. A custom printed-circuit board with four analog-to-digital conversion (ADC) channels was used to digitize the whole-cell patch-clamp signals. The ADCs were triggered with a sampling signal, derived from the same clock as used for the ADCs of the HD-MEA, so that signal synchronization between the HD-MEA and the patch-clamp signals was ensured.[43]

Statistics

Pearson correlation and two-side t-tests were done in Matlab R2014a (MathWorks).

Supplementary Material

Refer to Web version on PubMed Central for supplementary material.

Acknowledgements

D.J.B. and M.E.J.O. contributed equally to this work. This work was supported by the European Community through the European Research Council Advanced Grants 694829 “neuroXscales” (Horizon 2020) and 267351 “NeuroCMOS” (FP7), the Swiss National Science Foundation Grant 205321_157092/1 (“Axons”), the Asahi Glass Foundation, the Kayamori Foundation of informational science advancement AMED (JP18dm0307009), and the JSPS KAKENHI Grants 16K14191 and 26630089. The funders had no role in study design, data collection and analysis, decision to publish, or preparation of the manuscript. The authors thank the collaborators at ETHZ, Alexander Stettler for postprocessing CMOS chips, Felix Franke and Wei Gong for critical discussions, Jan Müller for technical support, and the D-BSSE staff for expediting experiments. Experimental design and data analysis were done by D.J.B., D.J., U.F., and M.E.J.O.; D.J.B., D.J., M.E.J.O., and M.R. performed experiments; technical support was provided by D.J.B., D.J., U.F., and M.R.; D.J.B., U.F., M.E.J.O., A.H., and H.T. wrote the manuscript; and project supervision was done by U.F., H.T., and A.H. All authors approved the final version of the manuscript.

References

[1]. Gold C, Henze DA, Koch C, Buzsaki G. J Neurophysiol. 2006; 95:3113. [PubMed: 16467426]

[2]. a)Pettersen KH, Einevoll GT. Biophys J. 2008; 94:784. [PubMed: 17921225] b)Holt GR, Koch C. J Computat Neurosci. 1999; 6:169.

[3]. Rall W. Biophys J. 1962; 2:145. [PubMed: 14490040]

[4]. Einevoll GT, Kayser C, Logothetis NK, Panzeri S. Nat Rev Neurosci. 2013; 14:770. [PubMed: 24135696]

[5]. Anastassiou CA, Perin R, Buzsaki G, Markram H, Koch C. J Neurophysiol. 2015; 114:608. [PubMed: 25995352]

[6]. Henze DA, Borhegyi Z, Csicsvari J, Mamiya A, Harris KD, Buzsaki G. J Neurophysiol. 2000; 84:390. [PubMed: 10899213]

[7]. Frey U, Egert U, Heer F, Hafizovic S, Hierlemann A. Biosens Bioelectron. 2009; 24:2191. [PubMed: 19157842]

[8]. Baranauskas G, David Y, Fleidervish IA. Proc Natl Acad Sci USA. 2013; 110:4051. [PubMed: 23341597]

[9]. Buzsaki G, Anastassiou CA, Koch C. Nat Rev Neurosci. 2012; 13:407. [PubMed: 22595786]

[10]. a)Grace AA, Bunney BS. Neuroscience. 1983; 10:317. [PubMed: 6633864] b)Petersen AV, Johansen EO, Perrier JF. Front Cell Neurosci. 2015; 9:429. [PubMed: 26578887]

[11]. Humphrey, DR, Schmidt, EM. Neurophysiological Techniques. Humana Press; New York: 1990. 1

[12]. Colbert CM, Johnston D. J Neurosci. 1996; 16:6676. [PubMed: 8824308]

[13]. Hu W, Tian C, Li T, Yang M, Hou H, Shu Y. Nat Neurosci. 2009; 12:996. [PubMed: 19633666]

[14]. Kole MH, Ilschner SU, Kampa BM, Williams SR, Ruben PC, Stuart GJ. Nat Neurosci. 2008; 11:178. [PubMed: 18204443]

[15]. Lorincz A, Nusser Z. Science. 2010; 328:906. [PubMed: 20466935]

[16]. Dodge FA, Cooley JW. IBM J Res Dev. 1973; 17:219.

[17]. Mainen ZF, Joerges J, Huguenard JR, Sejnowski TJ. Neuron. 1995; 15:1427. [PubMed: 8845165]

[18]. a)Kole MHP, Ilschner SU, Kampa BM, Williams SR, Ruben PC, Stuart GJ. Nat Neurosci. 2008; 11:178. [PubMed: 18204443] b)Leterrier C. J Neurosci. 2018; 38:2135. [PubMed: 29378864]

[19]. a)Leterrier C, Dubey P, Roy S. Nat Rev Neurosci. 2017; 18:713. [PubMed: 29097785] b)Schmidt-Hieber C, Bischofberger J. J Neurosci. 2010; 30:10233. [PubMed: 20668206] c)Hallermann S, de Kock CP, Stuart GJ, Kole MH. Nat Neurosci. 2012; 15:1007. [PubMed: 22660478]

[20]. Frey U, Sedivy J, Heer F, Pedron R, Ballini M, Müller J, Bakkum D, Hafizovic S, Faraci FD, Greve F, Kirstein KU, et al. IEEE J Solid-State Circuits. 2010; 45:467.

[21]. Obien ME, Deligkaris K, Bullmann T, Bakkum DJ, Frey U. Front Neurosci. 2014; 8:423. [PubMed: 25610364]

[22]. Tamamaki N, Yanagawa Y, Tomioka R, Miyazaki J, Obata K, Kaneko T. J Comp Neurol. 2003; 467:60. [PubMed: 14574680]

[23]. Triarhou LC. Front Neuroanat. 2014; 8:133. [PubMed: 25477788]

[24]. Thome C, Kelly T, Yanez A, Schultz C, Engelhardt M, Cambridge SB, Both M, Draguhn A, Beck H, Egorov AV. Neuron. 2014; 83:1418. [PubMed: 25199704]

[25]. a)Debanne D, Campanac E, Bialowas A, Carlier E, Alcaraz G. Physiol Rev. 2011; 91:555. [PubMed: 21527732] b)Popovic MA, Foust AJ, McCormick DA, Zecevic D. J Physiol. 2011; 589:4167. [PubMed: 21669974]

[26]. Foust A, Popovic M, Zecevic D, McCormick DA. J Neurosci. 2010; 30:6891. [PubMed: 20484631]

[27]. Yu Y, Shu Y, McCormick DA. J Neurosci. 2008; 28:7260. [PubMed: 18632930]

[28]. Palmer LM, Stuart GJ. J Neurosci. 2006; 26:1854. [PubMed: 16467534]

[29]. a)Höfflin F, Jack A, Riedel C, Mack-Bucher J, Roos J, Corcelli C, Schultz C, Wahle P, Engelhardt M. Front Cell Neurosci. 2017; 11:332. [PubMed: 29170630] b)Grubb MS, Shu Y, Kuba H, Rasband MN, Wimmer VC, Bender KJ. J Neurosci. 2011; 31:16049. [PubMed: 22072655] c)Rasband MN. Nat Rev Neurosci. 2010; 11:552. [PubMed: 20631711]

[30]. a)Hausser M, Stuart G, Racca C, Sakmann B. Neuron. 1995; 15:637. [PubMed: 7546743] b)Gentet LJ, Williams SR. J Neurosci. 2007; 27:1892. [PubMed: 17314285] c)Martina M, Vida I, Jonas P. Science. 2000; 287:295. [PubMed: 10634782] d)Herde MK, Iremonger KJ, Constantin S, Herbison AE. J Neurosci. 2013; 33:12689. [PubMed: 23904605]

[31]. Sloper JJ, Powell TP. Philos Trans R Soc B. 1979; 285:173.

[32]. Peters A, Proskauer CC, Kaiserman-Abramof IR. J Cell Biol. 1968; 39:604. [PubMed: 5699934]

[33]. Meyer G, Wahle P. J Comp Neurol. 1988; 276:360. [PubMed: 3192767]

[34]. Bakkum DJ, Frey U, Radivojevic M, Russell TL, Müller J, Fiscella M, Takahashi H, Hierlemann A. Nat Commun. 2013; 4

[35]. a)Martina M, Yao GL, Bean BP. J Comp Neurol. 2003; 23:5698.b)Korngreen A, Sakmann B. J Physiol. 2000; 525(Pt 3):621. [PubMed: 10856117]

[36]. Destexhe A, Bedard C. J Neurophysiol. 2012; 108:953. [PubMed: 22572946]

[37]. Logothetis NK. Nature. 2008; 453:869. [PubMed: 18548064]

[38]. a)McIntyre CC, Grill WM. Biophys J. 1999; 76:878. [PubMed: 9929489] b)Fried SI, Lasker AC, Desai NJ, Eddington DK, Rizzo JF 3rd. J Neuro-physiol. 2009; 101:1972.

[39]. Radivojevic M, Jäckel D, Altermatt M, Müller J, Viswam V, Hierlemann A, Bakkum DJ. Sci Rep. 2016; 6

[40]. Hedstrom KL, Xu X, Ogawa Y, Frischknecht R, Seidenbecher CI, Shrager P, Rasband MN. J Cell Biol. 2007; 178:875. [PubMed: 17709431]

[41]. Viswam, V; Obien, M; Frey, U; Franke, F; Hierlemann, A. IEEE Biomedical Circuits and Systems Conf.: Healthcare Technology; Piscataway, NJ: IEEE; 2018. 1

[42]. Blanche TJ, Swindale NV. J Neurosci Methods. 2006; 155:81. [PubMed: 16481043]

[43]. Jäckel D, Bakkum DJ, Russell TL, Müller J, Radivojevic M, Frey U, Franke F, Hierlemann A. Sci Rep. 2017; 7

Europe PMC Funders Author Manuscripts

Europe PMC Funders Author Manuscripts

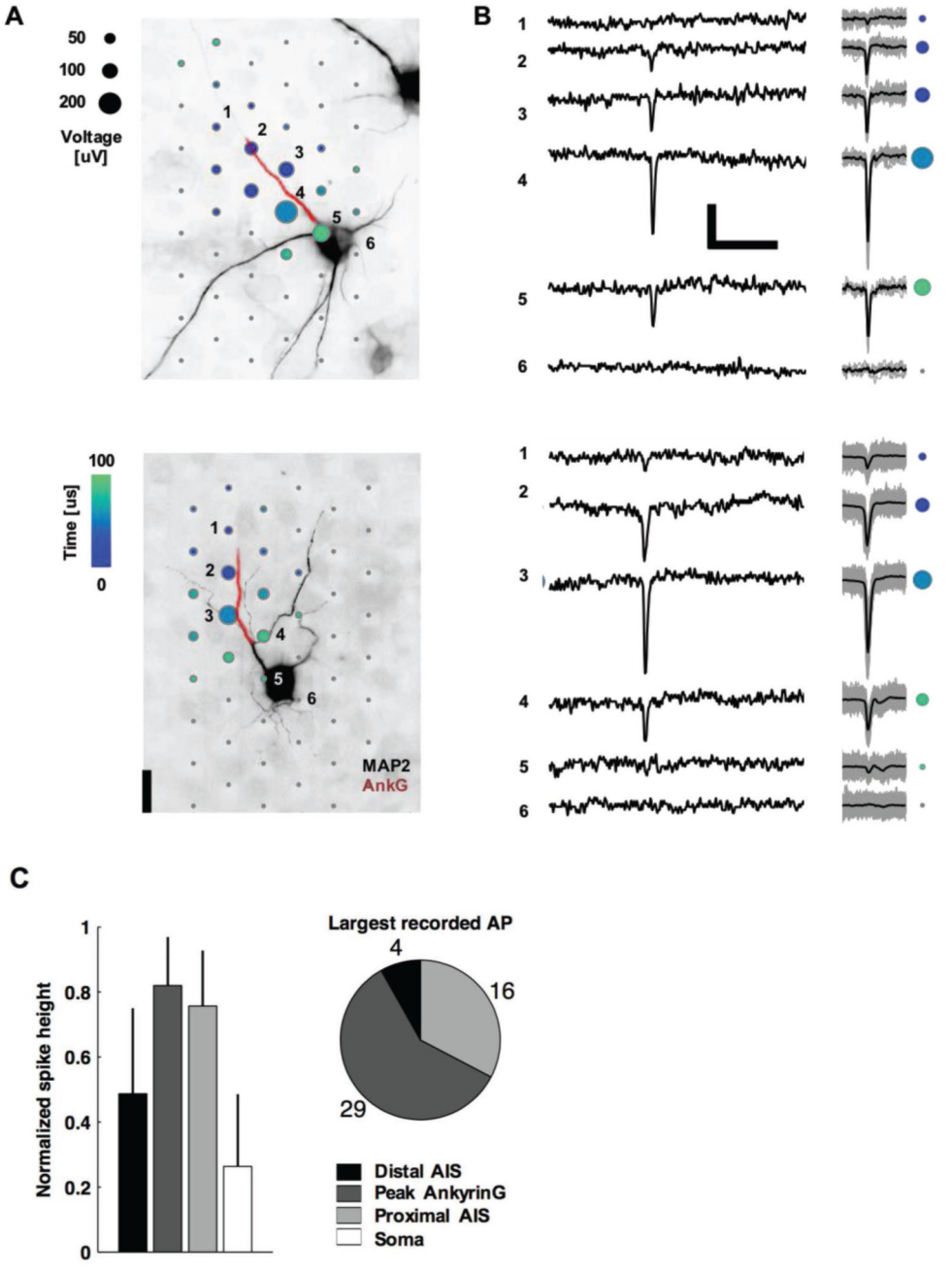

Figure 1. Neurons' negative-amplitude extracellular action potentials colocalize with their AISs.

A) Spatial and temporal (color) distribution of the averaged spontaneous extracellular action potential for two neurons. Dots are recording electrode locations, and dot sizes represent the AP negative peak voltage in the EAP, whereas the dot color represents the timing. The underlying fluorescence images show somas and dendrites (black; MAP2) and the AIS (red; AnkG). The EAPs are the average of 14 (top neuron) and 200 (bottom) spontaneous spikes. Numbered electrodes correspond to those in (B). Scale bar: 20 μm. B) Left: raw voltage waveforms of single action potentials; Right: overlay of multiple voltage waveforms (gray

lines; $N = 14$ top and 200 bottom) and averaged waveforms (black line) as used in (A). Colored dots correspond to those for the same electrodes numbered in (A). Scale bars: 100 μV and 5 ms. C) Summary statistics of negative spike heights. Data in the bar plots (mean ± s.d., $N = 49$) are normalized by the peak voltage amplitude in the EAP.

Europe PMC Funders Author Manuscripts

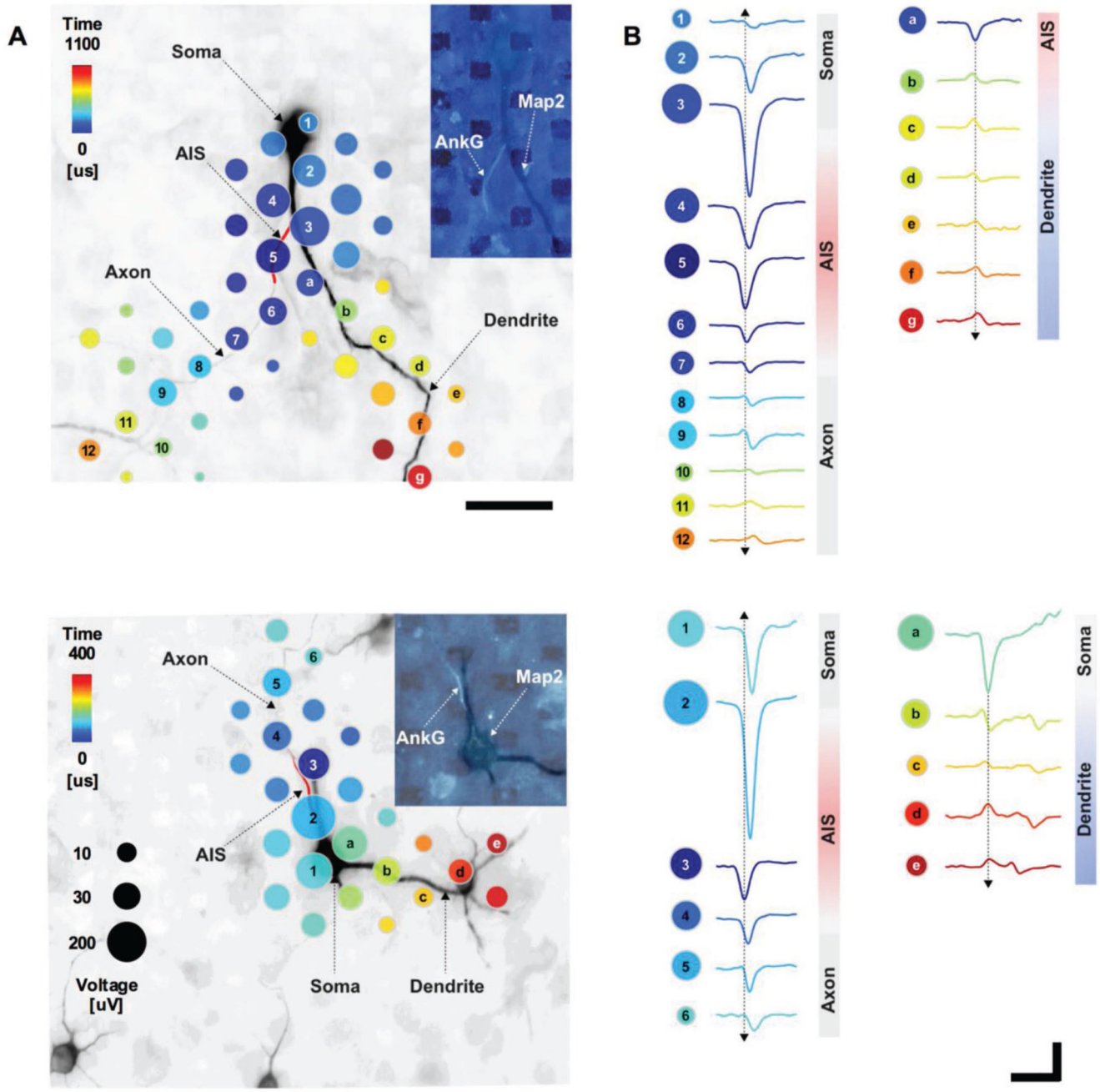

Figure 2. Detailed EAP.

A) Spatial and temporal distribution of the averaged spontaneous EAP for a neuron with an AIS originating from a dendrite (top) and an AIS originating from a soma (bottom). Dots mark recording-electrode locations. Time (dot color) is the delay from the first voltage peak, detected at the distal AIS, until the peak absolute voltage signal (dot size) at each location. Axonal and somatic areas correspond to signals that had larger negative peaks, while the dendritic area corresponds to signals that had larger positive peaks. The underlying fluorescence image shows somas, dendrites (black; MAP2), and the AIS (red cartoon;

AnkG). The inset fluorescence image shows MAP2 (dark) and AnkG (light); dark rectangles are electrodes. Scale bar: 50 μm. B) Average voltage waveforms recorded at the electrodes with matching labels to those in (A) (i.e., numbers and letters). Arrows indicate signal propagation direction. Scale bars: 100 μV vertical; 1 ms horizontal.

Europe PMC Funders Author Manuscripts

Europe PMC Funders Author Manuscripts

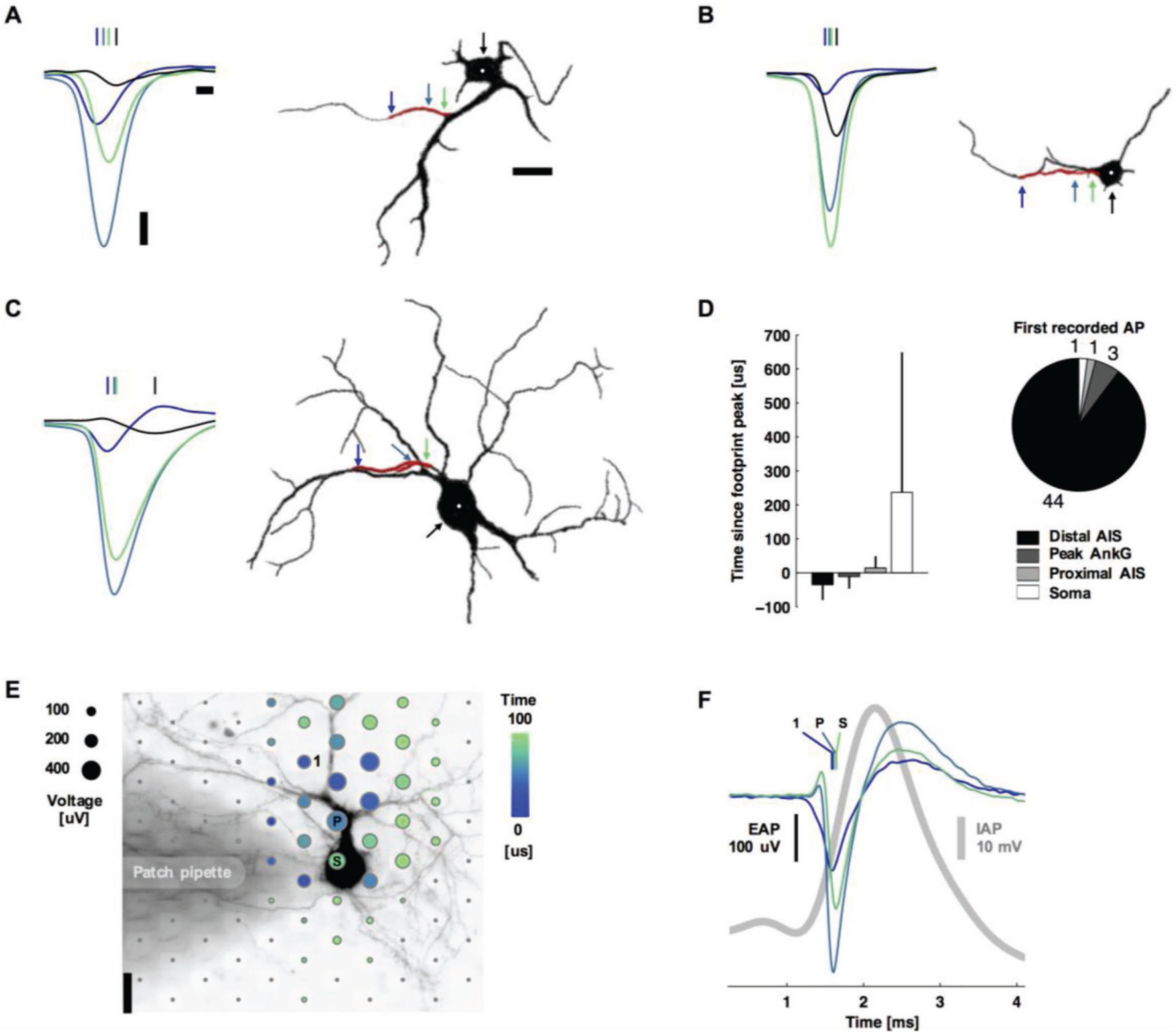

Figure 3. Action potentials typically initiated at the distal AIS.

A–C) Left: spontaneous action potentials at the distal AIS (blue), peak ankyrin-G fluorescence signal (blue-green), proximal AIS (green), and soma (black). Vertical lines indicate the timing of the negative voltage peak. Waveforms are the average of 11, 14, and 69 spikes for (A), (B), and (C). Right: silhouettes of immunostained neurons' fluorescence images (black: MAP2, red: ankyrin-G). Colored arrows and the white dot indicate the location of the plotted waveforms. Scale bars: 100 μV vertical; 100 μs left; 20 μm right. D) Summary statistics. Bar plots are mean ± s.t.d., $N = 49$. E) Spatial and temporal (color) distribution of the averaged EAP (dot sizes). The shaded area is a patch pipette that evoked action potentials by current injection and delivered the fluorescent dye for live-cell imaging. The labeled electrodes and waveform colors correspond to those in (B): the 1st electrode recording an action potential (1), the electrode recording the Peak voltage signal (P), and the electrode nearest to the Soma (S). Scale bar: 20 μm. F) Average intracellular (gray) and

extracellular (color) action potential waveforms (39 spikes). Colored vertical lines indicate the timing of the negative voltage peak.

Europe PMC Funders Author Manuscripts

Europe PMC Funders Author Manuscripts

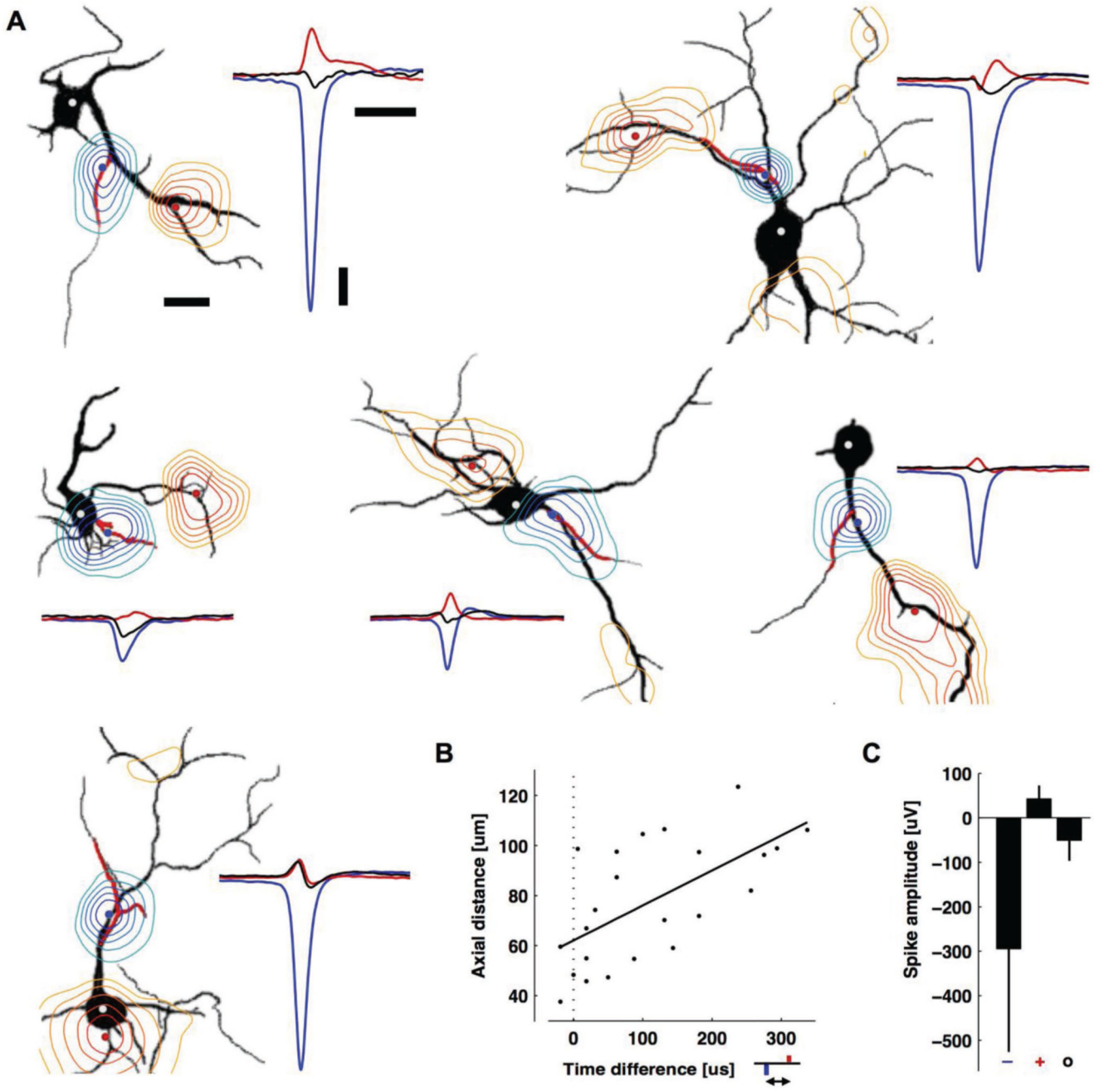

Figure 4. Positive-amplitude extracellular action potentials colocalized with some, but not all dendritic branches and occurred after the AIS spike.

A) Contour plots of the minimum (blue) or maximum (red) EAP within ± 500 μs of the negative peak (black silhouettes: MAP2, red: ankyrin-G). The background is an MAP2 fluorescence image with a drawn red line to indicate the AIS locations. The contours are normalized to the largest negative signal (blue-to-green) or the largest positive signal (red-to-yellow). The largest negative (blue) and positive signals (red) are also displayed as peaks at the right side of each panel along with the somatic potentials (black peaks). Adjacent contour lines then were drawn at 88%, 75%, 62%, 50%, and 38% of the respective peak

value for the negative signals (axonal blue-green), or 62%, 50%, 38%, 25%, and 12% of the respective peak value for positive signals (dendritic red-yellow). Scale bar: 20 μm. The blue, red, and white (soma) dots are the locations of the plotted waveforms. The two neurons in the top row are also in Figure 3. From left to right and top to bottom, EAPs are averages of 11, 69, 28, 68, 52, and 199 spontaneous spikes. Scale bars: 100 μV vertical; 1 ms right; 20 μm left. B) The time delay versus axial distance between the largest negative peak (blue) and the largest positive peak (red) voltages in the EAP. The line is a linear regression (Pearson's correlation coefficient $r = 0.79$, $p = 0.001$, $N = 24$). C) Average peak negative, peak positive, and somatic spike amplitudes (mean ± s.d., $N = 24$). Time courses of the EAPs can be seen in Movie S1 of the Supporting Information.

Europe PMC Funders Author Manuscripts

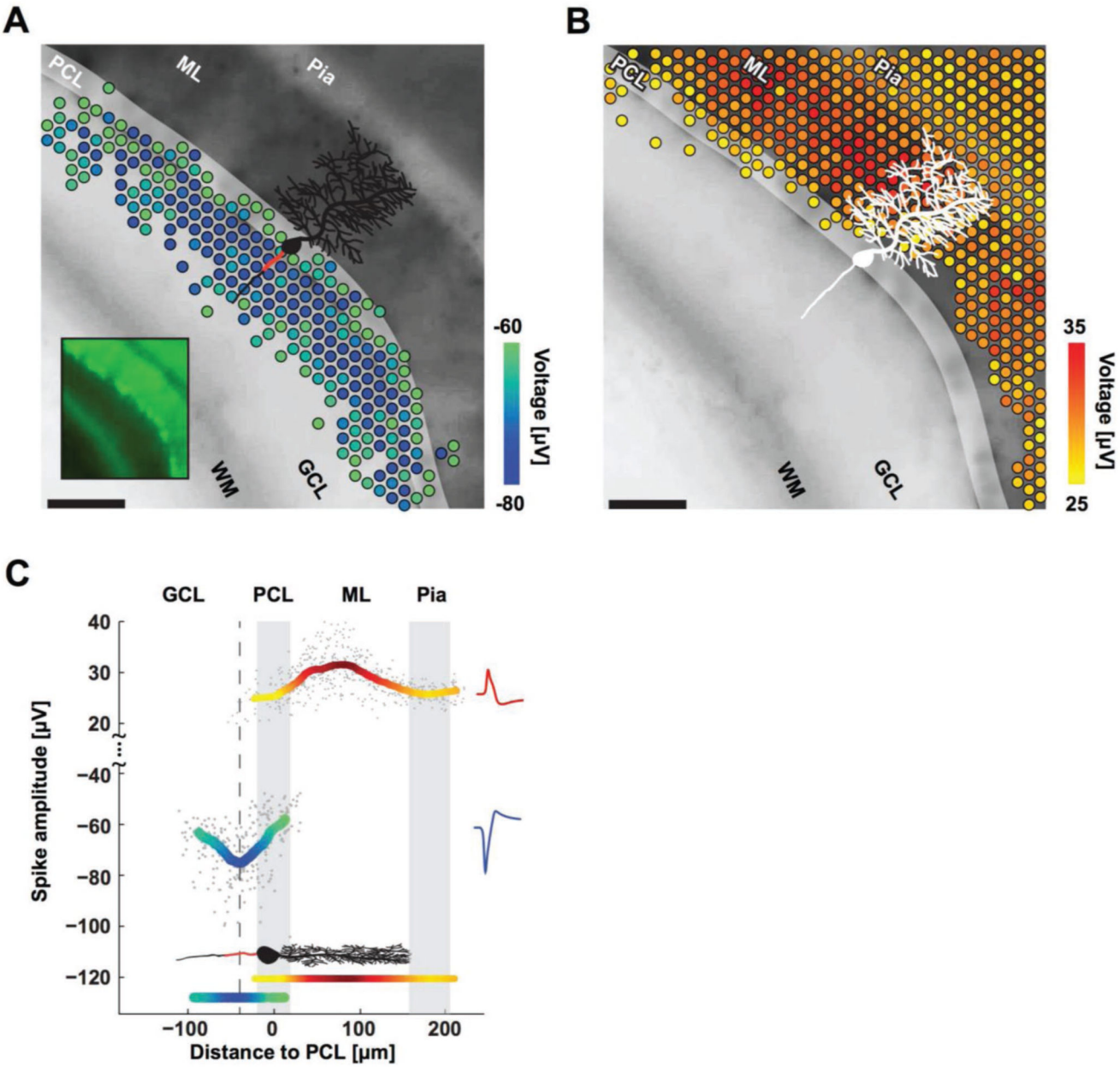

Figure 5. Purkinje cells' negative and positive EAPs colocalize with AISs and dendrites.

A) Spatial distribution of the most negative EAPs recorded from an acute cerebellar slice. Dots show the locations of recording electrodes that detect EAPs (color) below a –60 μV threshold. EAP amplitudes are the mean voltage of the 20 largest events during a 10 s recording. The underlying black-and-white live-cell fluorescence image, taken immediately after recording, shows the location of the cerebellar layers: white matter (WM), granular cell layer (GCL), Purkinje cell layer (PCL), molecular layer (ML), and pia. The somas of the Purkinje cells are in the PCL (highlighted for clarity; easier to see in the smaller inset image). All Purkinje cell dendrites are in the ML, all AISs are in the GCL. The microscopy image captured cells at the top layer of the acute slice, while the EAPs were recorded from

cells at the bottom layer. A sample cartoon of a Purkinje cell is shown in black with a red line estimating the AIS location. Scale bar: 100 μm. B) Distribution of the positive EAPs in analogy to A for EAPs above a 25 μV threshold. C) Summary of EAP amplitudes. Gray dots represent the largest negative or positive EAP amplitudes detected at each electrode versus the distance of the electrode from the PCL. Colored curves represent the mean for both negative (blue-green) and positive (yellow-red) EAPs as measured by the respective electrodes. The minimum in the curve representing the negative EAPs (dashed line at −40 μm) colocalizes with the putative location of AISs (red line in the cartoon of a Purkinje cell) in the GCL. The largest positive EAPs colocalize with the dendrites in the ML. Representative spike shapes of the negative (blue) and positive (red) EAPs, recorded from the acute cerebellar slice, are shown on the right.

Europe PMC Funders Author Manuscripts

Europe PMC Funders Author Manuscripts

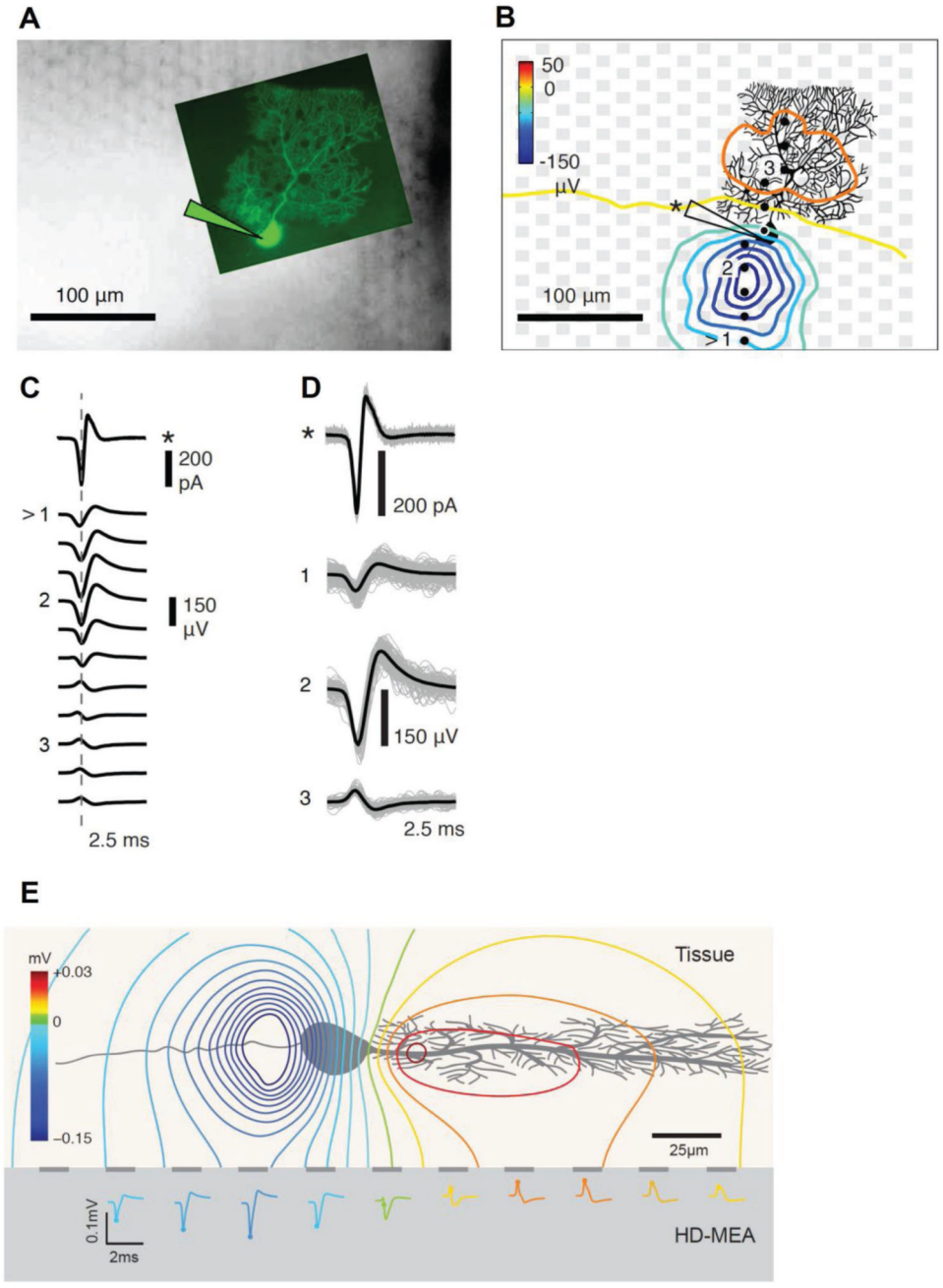

Figure 6. Combined cell-attached patch-clamp and high-density microelectrode array (HD-MEA) measurements show that the largest negative EAP of a Purkinje cell (PC) does not colocalize with the soma.

A) Fluorescence microscopy image of a measured Purkinje cell (PC), injected with Lucifer yellow, which was superimposed on an infrared differential-interference-contrast-microscopy image of the HD-MEA with an acute cerebellar slice with the focus on the electrode plane. B) Spatial distribution of the averaged spontaneous EAP of the Purkinje cell. The EAPs of the PC were extracted from HD-MEA recordings, while the timing of the action potentials has been obtained through cell-attached patch-clamp. The gray squares

indicate the electrodes, while the recorded PC is displayed in black. The yellow line marks the border between the molecular layer (ML) and the Purkinje cell layer (see also Figure 5A). The black dots represent the locations of the electrodes from which the waveforms in (C) were obtained. The largest EAP amplitudes were found along the axon of the PC. C) Averaged action potential waveforms of a PC simultaneously obtained through cell-attached patch-clamp (marked with *) and extracted from the electrode array as EAP waveforms along the string of marked electrodes from the bottom to the top in (B). The arrow symbol (>) marks the beginning of the string of electrodes at the bottom. D) Averaged waveforms of three electrodes (labeled 1–3) and the patch-clamp measurement displayed in (C) superimposed on the detected individual traces of action potential currents (*) and EAPs. E) Side-view schematic of the estimated extracellular potential distribution of a PC in an acute tissue placed on top of an HD-MEA. The estimated EAP distribution and waveforms on the HD-MEA electrodes are shown.

Europe PMC Funders Author Manuscripts